Applied Catalysis B: Environmental 111–112 (2012) 476–484

Contents lists available at SciVerse ScienceDirect

Applied Catalysis B: Environmental

journal homepage: www.elsevier.com/locate/apcatb

Synchrotron radiation PXRD investigation of V_2O_5/TiO_2 catalysts for 1,2-dichlorobenzene oxidation: Implication of structure modification

Hsi-Yan Chang[c], Shao-Pin Wang[c], Jen-Ray Chang[d], Hwo-Shuenn Sheu[b,**], Shin-Guang Shyu[a,*]

[a] Institute of Chemistry, Academia Sinica, Nankan, Taipei, Taiwan
[b] National Synchrotron Radiation Research Center, Hsinchu, Taiwan
[c] Department of Chemistry, National Cheng Kung University, Tainan, Taiwan
[d] Department of Chemical Engineering, National Chung Cheng University, Chia-Yi, Taiwan

ARTICLE INFO

Article history:
Received 16 June 2011
Received in revised form 25 October 2011
Accepted 29 October 2011
Available online 6 November 2011

Keywords:
Oxidation reaction
PXRD
FT-IR
1,2-Dichlorobenzene
Rietveld refinement
V_2O_5/TiO_2

ABSTRACT

V_2O_5/TiO_2 catalysts were prepared by depositing vanadia on nano-particles of anatase TiO_2 and tested for oxidation of 1,2-dichlorobenzene. Activity of the catalyst can be enhanced by adding MoO_3 to the catalysts and introducing sulfur-containing compounds to the reaction system. Kinetic studies indicate that addition of MoO_3 reduces the apparent activation energy slightly and increases the pre-exponential factors at reaction temperatures higher than 350 °C; in contrast, introduction of sulfur-containing compounds only increases the pre-exponential factors. XRD and FT-IR results indicate that MoO_3 disperses vanadia species and induces formation of crystalline MoV_2O_8 during the reaction, whereas introduction of sulfur-containing compounds leads to no significant structure change. Based on these characterizations and analyses of the kinetic results, we suggest that increased catalyst acidity results in higher pre-exponential factors, while structure change in vanadia species leads to reduction in apparent activation energy.
© 2011 Elsevier B.V. All rights reserved.

1. Introduction

V_2O_5/TiO_2 catalysts have long been used in the fine chemical industry [1–6] and in air pollution control [7–11]. Recent reports show that the addition of molybdenum oxides species to the catalysts causes dramatic changes in the catalytic behavior of the catalysts, most important, by improving the catalyst activity [12–19]. However, the role of molybdenyl oxides in these catalysts is still not well understood because of the difficulty in structure characterization.

Three explanations have been proposed for the roles of molybdenyl oxides (MoO_x). First, MoO_3 prevents TiO_2 sintering upon vanadia addition [12]. Second, the addition of MoO_x may cause the electronic interactions between the TiO_2-supported V_2O_5 and MoO_x leading to an increase of vanadia reducibility [13], thereby decreasing the energy barrier for reaction. Third, molybdenum oxides induce positive charges [12] leading to a generation of extra acid sites [17–19], thereby enhancing the reactant adsorption. In order to distinguish between the last two suggested roles, test reactions were carried out under sulfur-oxides free and sulfur-oxides containing environment at temperature TiO_2 sintering could not occur. In the presence of sulfur oxides, the acidity of the catalysts was expected to be increased with the adsorption of SO_x on the catalyst surface [17–19]. If the effects of MoO_x addition on the reaction kinetics are similar to that of SO_x adsorption, the increase of catalyst acidity may be suggested to be the main role of MoO_x addition [17–19]. Otherwise, change of vanadia reducibility may play a role in the activity enhancement.

Catalysts were tested by the oxidation of 1,2-dichlorobenzene because it has similar reaction behavior to dioxins, and dioxins formed in the waste incinerator during the combustion process have a serious impact to environment [20,21]. In addition, V_2O_5/TiO_2 is a commercial dioxin-oxidation catalyst, and fundamental understanding the catalytic chemistry allows us to improve the catalysts. Recent reports showed that chlorinated aromatics are not so well to be used to imitate polychlorinated dibenzo-p-dioxins (PCDD) and polychlorinated dibenzofurnas (PCDF) [22–24]. Oxygenated VOC could be a better model compound than 1,2-dichlorobenzene, and gas stream containing PCDD and PCDF was used directly to test the catalytic activities of the catalyst. Nevertheless, 1,2-dichlorobenzene was still chosen in our study because it is a classical choice and its toxicity is much lower [20,21,25].

Synchrotron powder X-ray diffraction (PXRD), which presents a much higher signal to noise ratio than laboratory PXRD and allows us to estimate structure parameters, crystallite size, and percentage of different phase in the catalyst samples, was used to characterize

* Corresponding author. Tel.: +886 2 27898592; fax: +886 2 27831237.
** Corresponding author. Tel.: +886 3 5780281; fax: +886 3 5783813.
E-mail addresses: hsheu@nsrrc.org.tw (H.-S. Sheu), sgshyu@chem.sinica.edu.tw (S.-G. Shyu).

0926-3373/$ – see front matter © 2011 Elsevier B.V. All rights reserved.
doi:10.1016/j.apcatb.2011.10.037

the catalyst structure. Acidity and vanadia reducibility of the catalysts were characterized by pyridine adsorption FT-IR and temperature programmed reduction (TPR), respectively. The roles of MoO_x addition were suggested by the correlation of structure information, surface acidity and catalyst reducibility with the kinetic study.

2. Experimental

2.1. Catalyst preparation

The samples were prepared by incipient-wetness impregnation technique. TiO_2 nano-particles (Merck, surface area of 40 m^2/g, average crystal grain size <100 nm) were pre-dried in an oven at 120 °C for 24 h remove the water. $(NH_4)_6Mo_7O_{24}{\cdot}4H_2O$ (3.28 g; ammonium molybdate powder, WAKO Pure Chemical) and 2.11 g citric acid was dissolved in 50 mL de-ionized water. Titanium dioxide (9 g) was brought in contact with the aqueous molybdate solution. The water solvent was removed by evacuation for 4 h at room temperature, and the resulting solid was calcined under air at 450 °C for 4 h. The sample after the calcination was noted as MoO_3–TiO_2.

MoO_3–TiO_2 and TiO_2 supports were dried under vacuum at 120 °C for 12 h. Two portions of solution by dissolving vanadium (V) oxide (0.735 g) and oxalic acid (2.52 g) in 10 mL of de-ionized water with stirring for 3 h were prepared. MoO_3–TiO_2 (9 g) was added to one portion, and TiO_2 support was added to the other. After calcinations at 450 °C in flowing air for 3 h, the samples were noted as V_2O_5/MoO_3–TiO_2 (VMoT) and V_2O_5/TiO_2 (VT). All samples were stored in a nitrogen-filled glove box before synchrotron PXRD and FT-IR spectroscopy measurement.

The compositions of vanadium, titanium and molybdenum were measured by inductively plasma optical emission measurement (ICP-OES, Perkin Elmer PE Optima 4300) in China Steel Corporation. The vanadium contains for VT and VMoT are 3.8 and 3.9 wt% respectively. The weight fractions of Mo in MoO_3–TiO_2 and VMoT are 15.0 and 13.8 wt%, respectively. The EDS results are in good agreement with those measured by ICP.

2.2. Activity measurements

The catalysts were tested in a stainless steel, single-pass, fixed bed reactor with an inside diameter of 2.2 cm and length of 45 cm. Powder VT and VMoT samples were pressed into 2–4 mm pellets. The reactor was heated electrically and temperature controlled by a PID temperature controller with three K-type thermal couples at the outer wall of the reactor. The reactor was packed with 2.0 g catalyst mixed with inert ceramic (sphere of about 0.5–1.0 mm diameter) in a ratio of 1:10 by volume, and a gradient packing method was used so that the catalyst bed would have a nearly uniform temperature, and the wall and bypassing effects would be minimized. For sulfur-oxides free environment, 1,2-dichlorobenzene (Aldrich, 99%) at weight hourly space velocity (WHSV) of 0.2 g of feed/(h × g) of catalyst and air at flow rate of 250 mL/min were metered into the reaction system by a LC pump and mass flow controllers, respectively. For sulfur-oxides containing environment, the feed was dry 1,2-dichlorobenzene containing 200 ppm sulfur with thiophene as the model sulfur compound. The oxidation reactions were carried out under atmospheric pressure with temperature ranged from 200 to 550 °C. Water, unreacted 1,2-dichlorobenzene and species formed from partial oxidation were trapped by a condenser at −5 °C. Samples were collected periodically and analyzed by GC (Shimadzu Model GC-14B with a FID and a TCD detectors) and GC/mass spectrometer (Shimadzu Model GC-17A-GCMS: QP5050(A)). Both spectrometers were equipped with a BP1 (100% dimethyl polysiloxane) capillary column, and were operated at 40–200 °C with ramping rate of 10 °C/min and a flow rate of 50 mL/min of dry He. CO and CO_2 were analyzed by GC equipped with a unibeads packed column of 3 m × 3 mm i.d. with a TCD detector. About 96% of the feed was recovered as reaction products as estimated by material balance calculations. The 4% loss is attributed to hydrocarbon deposited on the wall of reaction system, both on the catalyst and on the surface of ceramic packing. After the test reactions, the catalysts were unloaded from the reactor for characterization after purging with nitrogen to remove adsorbed hydrocarbon and water. The unloaded VMoT catalyst samples were noted as UVMoT and SUVMoT for reactions under sulfur-oxides free and sulfur-oxides containing environment, respectively, and the unloaded VT catalyst samples were noted as UVT and SUVT.

2.3. Synchrotron PXRD

Powder X-ray diffraction was performed at the BL01C2 beamline of the National Synchrotron Radiation Research Center (NSRRC), with the wavelength of 0.9535 Å (13.0 keV). The ring of NSRRC was operated at energy 1.5 GeV with a typical current 300 mA with top-up injection mode. The synchrotron X-ray was produced from a 5.0 T superconducting wavelength shift magnet. Beyond the pre-focusing mirror, a double crystal monochromator, which used the Si (1 1 1) plane to yield the monochromatic beam, was followed by a refocusing toroidal mirror. Sample was sealed in capillary. During the X-ray exposure, the sample was kept fast spin in order to increase the orientations of powders. Two-dimensional diffraction patterns were recorded by a Mar345 imaging plate system, with a sample-to-detector distance of 300 mm. Diffraction angle 2θ was calibrated with silver Behenate and Si powders (NBS640b) standards. One-dimensional PXRD profiles were integrated from selected fan-like areas of the symmetrical 2-dimensional powder rings using the Fit2D program [26]. Crystal structure parameters were refined with the Rietveld method [27] using the graphical interface package EXPGUI [28] for GSAS program [29], and the crystalline grain sizes were obtained from the commonly used Scherrer's equation $t = k\lambda/(B\cos\theta)$ [30], with the crystal grain size t, shape correction constant $k = 0.95$ for spherical particle, and FWHM of the related Bragg peaks B.

2.4. FT-IR spectroscopy

Diffuse reflectance infrared Fourier transform spectra (DRIFT) of fresh and used VMoT and VT samples were recorded with Shimadzu FT-IR IRPrestige-21, having a spectral resolution of 2 cm^{-1}. The powder samples were loaded into the DRIFT. The cell was connected to a vacuum/gas-handling manifold for in situ treatment. For the characterization of vanadia species on TiO_2 and MoO_3–TiO_2 supports, KBr was loaded into the DRIFT cell, and background IR spectra was taken. The catalyst and support samples were then loaded into the DRIFT cell, and IR spectrum were recorded.

For FT-IR characterizing pyridine adsorbed on catalysts, samples were purged with dry N_2 at room temperature for 1 h and followed with the evacuation to a pressure of approximately 10^{-2} Torr. After taking the background IR spectra, pyridine was introduced into the IR cell and maintained for about 20 min for pyridine adsorption. The cell was then evacuated to a pressure of approximately 10^{-2} Torr, and IR spectra for pyridine adsorption were recorded.

2.5. Temperature programmed reduction (TPR)

The apparatus used for the TPR studies was described by Jones and McNicol [31]. A gas stream of 10% H_2 in argon passed through the fresh and used catalysts in a quartz reactor heated at 10 °C/min to 700 °C with a temperature-programmed furnace. The amounts

of H_2 consumed in reduction were detected with a thermal conductivity detector (TCD) and the reduction temperature was monitored by a thermocouple.

3. Results and discussion

3.1. Catalytic performance

Oxidation of 1,2-dichlorobenzene was carried out in a fixed bed reactor with air under atmospheric pressure. The reactions were tested in both sulfur free and sulfur containing environments. The total oxidation selectivity of 1,2-dichlorobenzene for CO_2 was up to 95%. The major by-products (e.g. 4-methylpent-3en-2one, hex-5-en-one, and 4-hydroxyl-4-methylpentan-2-one) were formed from the partial oxidation of 1,2-dichlorobenzene. Trace by-products such as 1,2,3- and 1,3,5-trichlorobenzene were formed in trace amount (less than 500 ppm) through chlorination of 1,2-dichlorobenzene. The conversion of 1,2-dichlorobenzene and the selectivity to CO_2 as a function of reaction temperature are shown in Fig. 1a and b, respectively. The relative conversion and selectivity to CO_2 decreased in the order of VMoT (S) > VMoT > VT (S) > VT, where (S) represents the reaction operated under sulfur-oxides containing environment. Since no thiophenes have been detected by GC, we suggested that the compound was totally converted to sulfur oxides (SO_x) under reaction conditions. Sulfur oxides adsorbed on the catalysts increases the acidity of the catalysts, leading to an increase of catalyst conversion and selectivity [17–19]. The adsorption of SO_x was evidenced by FT-IR characterizing the used catalysts.

In order to demonstrate the promoting effects of the addition of MoO_3, The catalytic properties of MoO_3–TiO_2 support has also been tested and the results indicated that DCB conversion is insignificant at temperature lower than 400 °C. The results indicate that the higher activity for VMoT as opposed to VT is contributed from the promoting effects of MoO_3 [17–19]; the addition of MoO_3 in VT change the morphology of vanadia, which is the active sites for oxidation reaction.

Assuming oxidation of 1,2-dichlorobenzene occurs through a rate determining surface reaction [32], in large excess oxygen, the rate expression can be formulated as:

$$\text{Rate} = \frac{-ks \times K_{DCB} \times [DCB]}{1 + K_{po} \times [PO] + K_{DCB} \times [DCB]} \quad (1)$$

where DCB, PO, *ks* and *K* denote 1,2-dichlorobenzene, partial oxidation by-products, surface reaction rate constant and adsorption equilibrium constant, respectively.

The electron lone pairs on the oxygen atom of carbonyl or hydroxyl group, chlorine atom of the aromatic chloride and even the pi-electron of the olefin group or aromatic pi-electrons in the partial oxidation products may act as Lewis base. These electron lone pairs or pi-electrons coordinate to the acidic sites (both Lewis acid and Brønsted acid) of the catalyst furnishing the absorption step of the catalytic reaction.

At reaction temperatures higher than 350 °C, the adsorption of 1,2-dichlorobenzene and partial oxidation by-products on active sites are small and the adsorption equilibrium terms, $K_{po} \times [PO]_x$ and $K_{DCB} \times [DCB] \ll 1$. Thus, the over-all rate expression can be simplified as:

$$\text{Rate} = -ks \times K_{DCB} \times [DCB] = k \times [DCB] \quad (2)$$

This rate expression is consistent with the pseudo 1st order kinetics proposed by Amiridis et al. [20,21,33]. The rate constant *k* for the reaction is composed of two terms, *ks* (surface reaction rate constant) and the K_{DCB} (adsorption equilibrium constant of 1,2-dichlorobenzene).

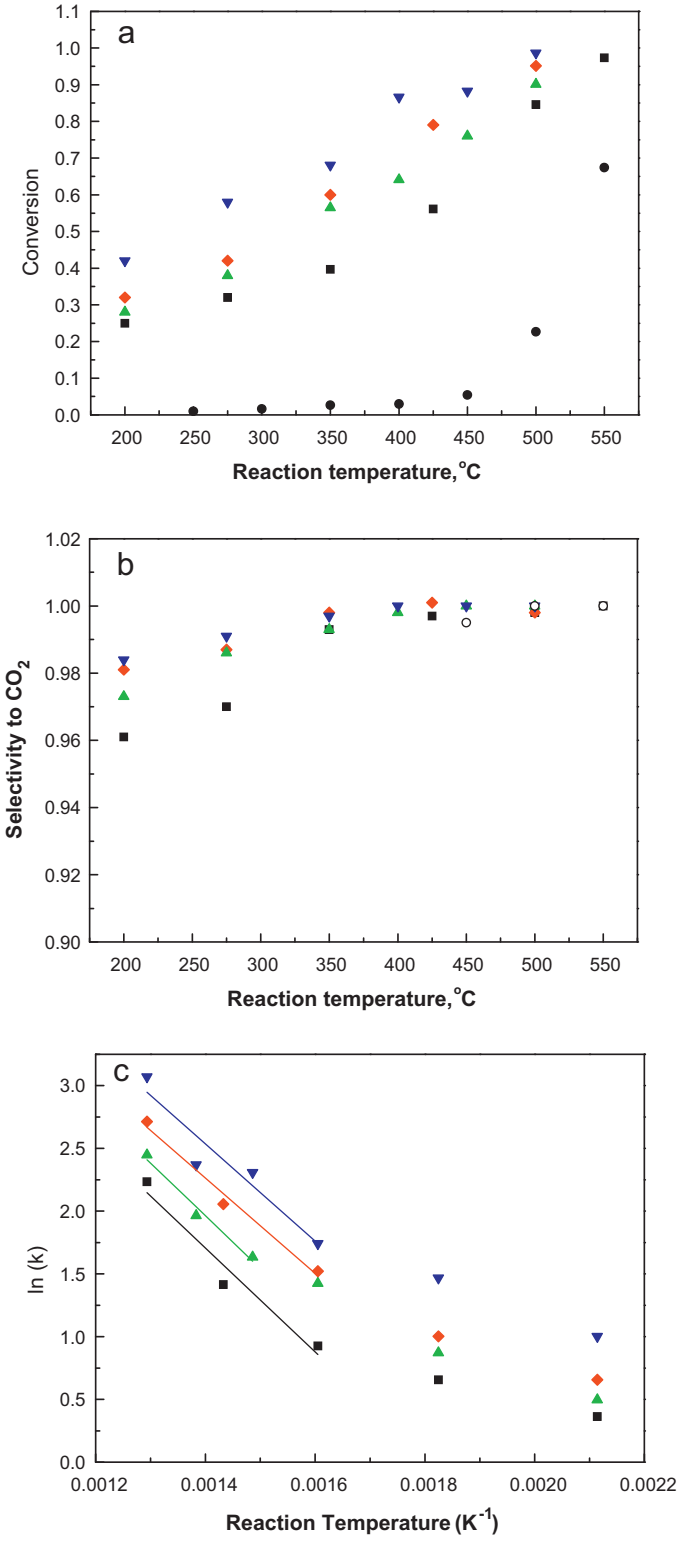

Fig. 1. (a) 1,2-Dichlorobenzene conversion as a function of temperature, (b) selectivity to CO_2 as a function of temperature, and (c) Arrhenius plots for 1,2-dichlorobenzene conversion for: (▼) VMoT under sulfur oxides environment; (♦) VMoT under sulfur-oxides free environment; (▲) VT under sulfur-oxides environment; (■) VT under sulfur oxides free environment; (●) M_2O_3–TiO_2 under sulfur oxides free environment.

Table 1
Apparent activation energies and frequency factors for oxidation of 1,2-dichlorobenzene catalyzed by VT and VMoT under sulfur oxide free and sulfur containing environments at temperature higher than 400 °C.

Catalyst	*ko*	*Ea* (kJ)
VT	1826	34.4
VMoT	1958	31.5
VT(S)	2565	35.0
VMoT (S)	2836	32.2

The temperature dependence *ks* and K_{DCB} are formulated as:

$$ks = ks^0 \exp\left(\frac{-Es}{RT}\right) \quad \text{and} \quad K_{DCB} = K^0_{DCB} \exp\left(\frac{-Ha}{RT}\right) \tag{3}$$

where ks^0 is the pre-exponential factor of Arrhenius equation and K^0_{DCB} is the heat of reaction in the standard state. The lumped rate constant *k* is formulated as:

$$k = ks \times K_{DCB} = ks^0 \exp\left(\frac{-Es}{RT}\right) \times K^0_{DCB} \exp\left(\frac{-Ha}{RT}\right)$$
$$= ks^0 \times K_{DCB} \exp\left(\frac{-(Ha+Es)}{RT}\right) = k^0 \times \exp\left(\frac{-Eapp}{RT}\right) \tag{4}$$

Thus, apparent activation energy can be formulated as Eapp = *Es* (activation energy of surface reaction) + *Ha* (adsorption heat of 1,2-dichlorobenzene).

Based on the pseudo 1st order kinetics, the activation energy (Eapp) and the frequency factor (pre-exponential term, k_0) were estimated by the Arrhenius plots (Fig. 1c, Table 1). The result indicates: (1) adsorptions of 1,2-dichlorobenzene and partial oxidation by-products decrease with increasing reaction temperature, (2) introduction of thiophene to reaction system increases the pre-exponential factors, and (3) the utilization of MoO_3–TiO_2 supports decreases the apparent activation energy and slightly increase pre-exponential factors.

The accuracy of apparent-activation estimation is based on the justification of the assumption that $K_{DCB} \times [DCB] \ll 1$ at high temperature. The process of DCB adsorption is exothermic and the amount of DCB adsorbed on the catalyst decreases with increasing reaction temperature. Hence, the conclusion regarding the role of MoO_3 in decreasing apparent-activation is true at rather high temperature. Unfortunately, Arrhenius plots are unable to give us the exact temperature that the DCB adsorption factor is unimportant.

3.2. PXRD data analysis

PXRD patterns of VT before and after test reactions were shown in Fig. 2. Anatase TiO_2 supports and V_2O_5 formed on the supports are very stable. After test reactions, no phase changes were observed. In contrast, amorphous vanadia species formed on MoO_3–TiO_2 supports are relatively unstable. During test reactions, MoV_2O_8 crystals were formed by the reaction of amorphous vanadia with MoO_3 (Fig. 3). In order to fully characterize the structure of surface species formed on the anatase supports, Rietveld refinement method was applied on the analysis of diffraction data which contain majority of known structural information with minor modifications of structures or chemical compositions. Rietveld method is one of the most important methods to quantitatively investigate each component in multi-phase crystalline sample.

The method was first developed to refine crystal structure based on full diffraction profile analysis by Rietveld in 1969 [27]. The powder X-ray diffraction pattern was converted to the typical step width of 0.02° in 2θ. Y_i represents the diffraction intensity at step i

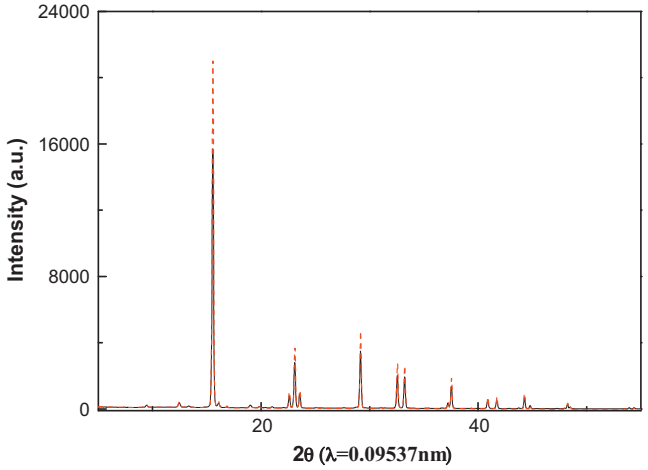

Fig. 2. Powder X-ray diffraction patterns of (a) VT (black solid line) and (b) UVT (red dashed line). (For interpretation of the references to color in this figure legend, the reader is referred to the web version of the article.)

that may contain contributions from several Bragg reflections, such as:

$$Y_i = s\Sigma_k M_k L_k |F_k|^2 P(\theta_i - \theta_B) O_k + Y_{ibck} \tag{5}$$

where *s* is a scale factor; Σ_k means the sum over all *k* Bragg reflections; *M* is the multiplicity factor; *L* is the Lorentz and polarization factor; *F* is the structure factor; *P* is the profile function; θ_i is the diffraction angle of the i step; θ_B is the Bragg angle of reflection *k*; *O* is the preferred orientation function; and Y_{ibck} is the background at step i. During the refinement, the quantity to be minimized is the weighted sum of the squares of the differences between observed and calculated intensity at each step. This is

$$wR_p = \Sigma_i w_i |Y_{iobs} - Y_{ical}| / \Sigma_i (Y_{iobs}) \tag{6}$$

In this study, the diffraction data of crystallites were analyzed and refined by the Rietveld method using the GSAS-EXPGUI program [28,29]. The calculated diffraction profiles were based on Pseudo–Voigt (Gaussian plus Lorentzian) distribution and broad peak widths. It is noticeable that the diffraction patterns contain many crystalline phases. While applying the Rietveld refinement method to study these powder diffraction patterns, special care must be taken.

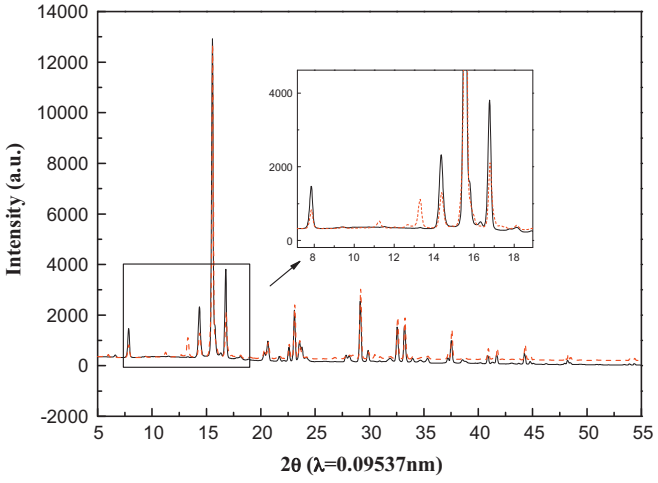

Fig. 3. Powder X-ray diffraction patterns of (a) VMoT (black solid line) (b) UVMoT (red dashed line). (For interpretation of the references to color in this figure legend, the reader is referred to the web version of the article.)

Table 2
Crystal data of Rietveld results for (a) VT, (b) UVT, (c) SUVT, (d) VMoT, (e) UVMoT, and (f) SUVMoT.

Chemical formula	TiO_2 (anatase)	V_2O_5
(a) VT		
Space group	$I4_1/amd$	Pmmn
a, Å	3.78472(3)	11.529(6)
b, Å	3.78472	3.5623(7)
c, Å	9.5132(47)	4.3844(7)
V	136.153(2)	180.08(3)
wR_p	0.0773	
R_p	0.0544	
χ^2	0.9648	
R_F^2	0.0435	
Weight fraction	0.951(5)	0.048(5)
Crystalline size, nm	40	27
(b) UVT		
Space group	$I4_1/amd$	Pmmn
a, Å	3.78380(3)	11.508(2)
b, Å	3.78380	3.5602(5)
c, Å	9.50982(12)	4.3761(6)
V	136.153(2)	179.30(4)
wR_p	0.0761	
R_p	0.0547	
χ^2	0.5736	
R_F^2	0.0399	
Weight fraction	0.955(1)	0.045(1)
Crystalline size, nm	40	30
(c) SUVT		
Space group	$I4_1/amd$	Pmmn
a, Å	3.78243(3)	11.507(2)
b, Å	3.78243	3.5595(5)
c, Å	9.50625(12)	4.3754(6)
V	136.004(2)	179.21(4)
wR_p	0.0738	
R_p	0.0527	
χ^2	0.5509	
R_F^2	0.0454	
Weight fraction	0.952(1)	0.048(6)
Crystalline size, nm	39	30
(d) VMoT		
Space group	$I4_1/amd$	Pbnm
a, Å	3.77877(5)	3.9608(2)
b, Å	3.7787	13.871(1)
c, Å	9.4987(2)	3.6974(2)
V	135.632(4)	203.14(2)
wR_p	0.0785	
R_p	0.0538	
χ^2	1.748	
R_F^2	0.0659	
Weight fraction	0.789(1)	0.211(2)
Crystalline size, nm	36	24

Chemical formula	TiO_2	MoO_3	MoV_2O_8	VO_2
(e) UVMoT				
Space group	$I4_1/amd$	Pbnm	C2	P2/m
a, Å	3.78362(5)	3.9612(3)	19.415(3)	9.046(7)
b, Å	3.78362	13.868(1)	3.6254(6)	5.792(4)
c, Å	9.5096(2)	3.6959(3)	4.1170(7)	4.561(4)
b,°			90.56(4)	91.81(10)
wR_p	136.138(4)	203.03(3)	289.77(7)	238.8(3)
R_p	0.0894			
χ^2	0.066			
R_F^2	1.329			
Weight fraction	0.759(1)	0.123(2)	0.108(3)	0.0096(2)
Crystalline size, nm	39	27	26	34
(f) SUVMoT				
Space group	$I4_1/amd$	Pbnm	C2	P2/m
a, Å	3.78730(5)	3.9676(4)	19.477(5)	9.122(8)
b, Å	3.78730	13.893(2)	3.6247(6)	5.825(5)
c, Å	9.5190(2)	3.7018(4)	4.1205(6)	4.713(6)
b,°			90.65(4)	90.18(12)
V	136.538(4)	204.05(3)	290.88(9)	250.5(3)
wR_p	0.0971			
R_p	0.0724			
χ^2	1.522			
R_F^2	0.0699			
Weight fraction	0.749(1)	0.123(8)	0.12(1)	0.0065(4)
Crystalline size, nm	39	26	25	32

3.3. Rietveld refinement results

The Rietveld refine results of the powder X-ray diffraction patterns for VT, UVT, and SUVT are shown in Fig. 4a–c respectively. The refined crystal data for these samples were shown in Table 2a–c. All samples contain two components with the major phase of anatase TiO_2 and a minor phase of V_2O_5. The unit cell dimensions and volumes for TiO_2 and V_2O_5 are similar to those in literature. The Rietveld refinement results shows that weight fractions of crystalline V_2O_5 are 4.8(5), 4.5(1), and 4.8(6) wt.% and the average V_2O_5 crystalline sizes are 27, 30, and 30 nm for VT, UVT, and SUVT, respectively. The total amounts of V measured by ICP are 3.8 and 3.9 wt% for VT and VMoT, respectively. In terms of V_2O_5, the weight fractions become 6.8 and 6.94 wt% for VT and VMoT, respectively. The difference between total amount (ICP measurement) and crystalline phase (Rietveld refinement) are considering as amorphous. These results suggests that vanadia species on the anatase TiO_2 are rather stable, and about 30 wt% of the vanadia species are in amorphous form (two-dimensional layer V_2O_5 or three-dimensional V_2O_5 clusters with particle size less than 1.5 nm are beyond the detection limitation of synchrotron PXRD).

Similar analysis of powder X-ray patterns of VMoT, UVMoT, and SUMoT were also carried out by using Rietveld refinement. The refinement results are shown in Fig. 4d–f. Final refined crystal data for these catalyst samples are shown in Table 2d–f. For the VMoT sample, 22 wt% of MoO_3 with crystalline size of 24 nm is estimated from the refinement, whereas no crystalline V_2O_5 phase was detected. The results suggest that all Mo precursors have been converted to MoO_3 crystal during the calcinations process, while amorphous V_2O_5 were anchored on the Mo–TiO_2 supports.

The powder X-ray diffraction pattern of UVMoT and SUVMoT are much complicated than that of VMoT. Because phases of TiO_2, MoO_3, MoV_2O_8, and VO_2 were identified in the powder patterns, four phase refinements corresponding to these phase were included in the Rietveld refinement. Some unidentified tiny peaks appearing in these two PXRD patterns may belong to various composition of vanadium oxide VO_x (x = 2–5) and were not included in the refinement. Refinement results shows that the weight fractions of TiO_2 MoO_3, MoV_2O_8, and VO_2 for the UVMoT sample are 0.759(1), 0.123(2), 0.108(3), and 0.0096(2), respectively. For the SUMoT sample, the corresponding weight factors are 0.749(1), 0.123(8), 0.12(1), and 0.0065(4). The formation of MoV_2O_8 during the oxidation of 1,2-dichlorobenzene suggests that MoO_3 has higher affinity to vanadia species as compared to TiO_2. However, the formation mechanism and slightly higher MoV_2O_8 formation rate in SO_x containing environment are still unclear.

3.4. FT-IR characterization of vanadia species on TiO_2 and MoO_3–TiO_2 supports

FT-IR spectra of V_2O_5 nano-particles of 40 nm crystalline size, vanadia catalysts, TiO_2, and MoO_3–TiO_2 supports are shown in Fig. 5a. There are no significant FT-IR characteristic peaks for TiO_2 supports. For MoO_3–TiO_2 supports, peaks at about 995, 910, and 830 cm^{-1} are assigned as terminal oxygen symmetry stretching mode υ_s(Mo=O), bridging oxygen asymmetry υ_{as}(Mo–O–Mo), and

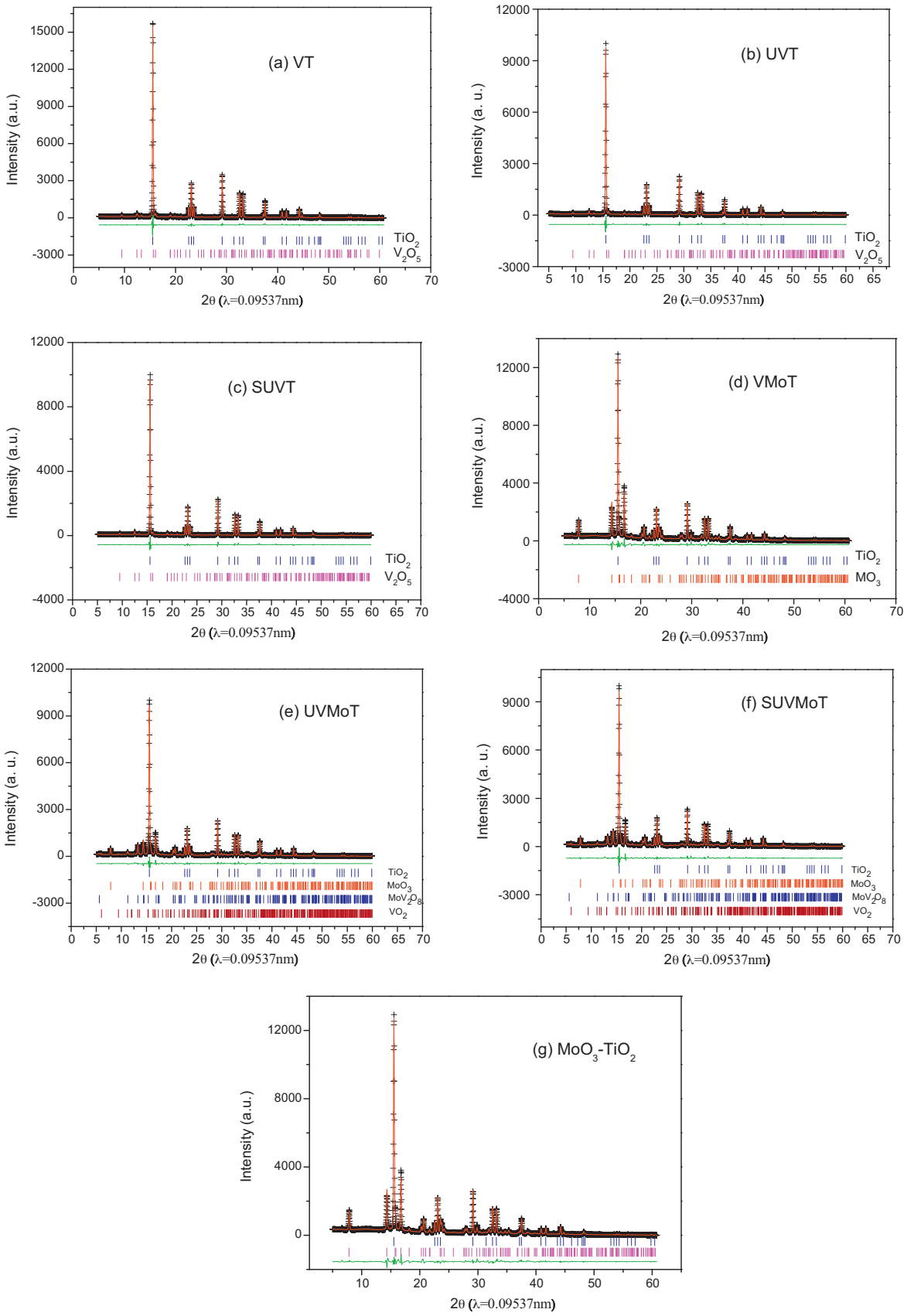

Fig. 4. Comparison of Rietveld refinement result (red curve) and experimental PXRD data (black daggers) of (a) VT, (b) UVT, (c) SUVT, (d) VMoT, (e) UVMoT, (f) USVMoT and (g) MoO_3–TiO_2. The green curve below illustrates the differences between data and simulation, whereas the short sticks mark the reflection positions of the tetragonal and orthorhombic phases for TiO_2 (blue), V_2O_5 (magenta), MoO_3 (red), MoV_2O_8 (navy), and VO_2 (brown) respectively. (For interpretation of the references to color in this figure legend, the reader is referred to the web version of the article.)

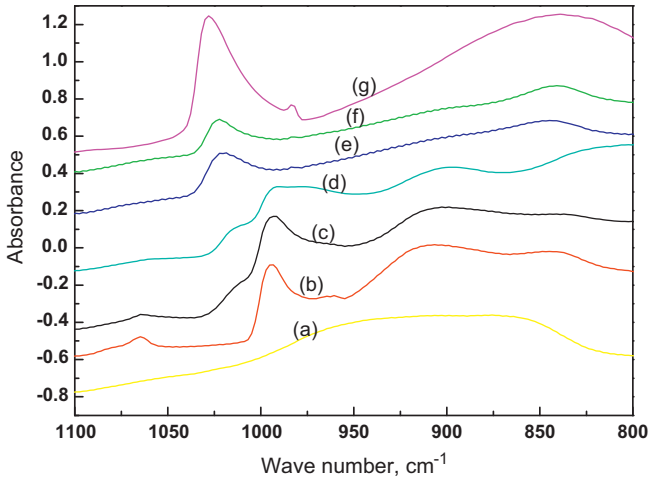

Fig. 5. FT-IR spectra of (a) TiO_2, (b) Mo_3–TiO2, (c) VMoT, (d) UVMoT, (e) VT, (f) UVT, and (g) V_2O_5 nano-particles.

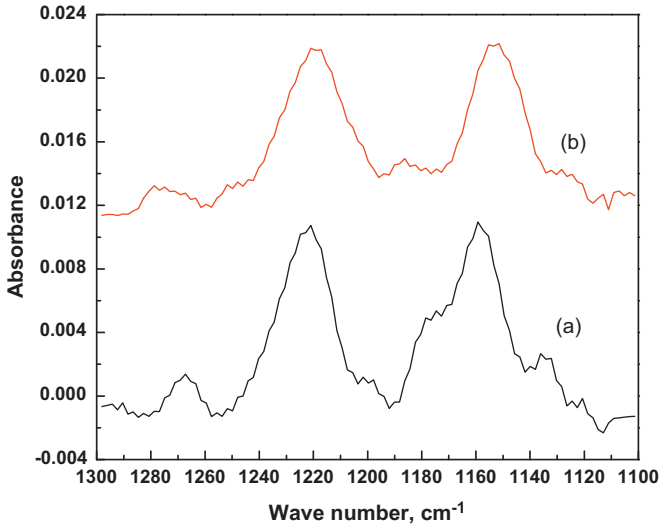

Fig. 6. FT-IR spectra characterizing sulfur species on (a) SUVT, and (b) SUVMoT.

bridging oxygen symmetry modes υ_s(Mo–O–Mo), respectively, of crystalline MoO_3 with Pbnm space group [34,35]. The interactions between MoO_3 and TiO_2 may be reflected in the shift of υ_s(Mo=O) from 995 to 1065 cm^{-1}. For V_2O_5 nano-particles, the strong and the weak peaks centered at about 1030 cm^{-1} is assigned as υ(V=O) stretching mode of crystalline V_2O_5 [36].

Based on Cavani et al. [10] the appearance of broad peaks at about 980 cm^{-1} is suggested to be originated from V=O bond stretching frequency for layer V_2O_5 on TiO_2. Both FT-IR spectra of VT and UVT show an absorption peak at 1020 cm^{-1} while no significant peak appears in the region of about 980 cm^{-1}. In comparison FT-IR spectra of V_2O_5 nano-particles, the shift of υ(V=O) to lower frequency suggests that on TiO_2 the particle size of V_2O_5 is smaller than that of V_2O_5 nano-particles whereas TiO_2–V_2O_5 interactions are insignificant because no significant peaks appear in the region of 980 cm^{-1}. By combined with Rietveld refinement results, we thus suggest that on TiO_2 supports, 65% is crystalline V_2O_5, and 35% is small 3-dimensional V_2O_5 with cluster size less than 2 nm.

Addition of Mo significantly alters the surface of VT. In comparison with the FT-IR spectra of VT, υ(V=O) further shifts to 1010 cm^{-1} for VMoT. The results suggest that V_2O_5 clusters on MoO_3–TiO_2 are smaller than those on TiO_2, consistent with the PXRD results. After the test reaction, the diminishing of the peak at 1065 cm^{-1} and the broadening of the peak at 995 cm^{-1} suggests that V_2O_5 reacted with MoO_3 during the test reaction. Rietveld refinement results further suggest that while over 90% of V_2O_5 was reacted with MoO_3 to form MoV_2O_8, small amount of layer and/or small V_2O_5 clusters were still intact during the test reactions.

FT-IR spectra characterizing the surface species on SUVT and SVMoT are shown in Fig. 6. Two main bands at about 1155 and 1220 cm^{-1} are the characteristic peaks for the stretching motion of adsorbed sulfate, SO_4^{2-}. The rather broad of these peaks could be due to several types of coordination environments or coordinates (monodentate and bidentate) to different type of metal oxides [37–39]. The adsorbed sulfate was formed by the reaction of sulfur oxides with water adsorbed on the metal oxides and the sulfur oxides was formed by the total oxidation of thiophene.

3.5. FT-IR characterizing pyridine adsorbed on catalysts

Pyridine adsorption (Py-ads) IR spectra characterizing the acidity of TiO_2 and MoO_3–TiO_2 supported vanadia catalyst samples are shown in Fig. 7. The IR spectra are consistent with the spectra reported [40–43] in the literature. The bands at 1635 and 1535 cm^{-1} are assigned to the adsorption of pyridine on Brønsted sites and the absorption peaks located at 1605 and 1445 cm^{-1} are assigned to the vibrational modes of pyridine coordinated to the Lewis acid sites. The band at 1490 cm^{-1} is suggested to be the contribution of the pyridine adsorbed on both Brønsted and Lewis sites.

Comparing the intensities of absorption bands in the Py-ads IR spectra characterizing TiO_2 and VT, the acid sites of VT catalysts are regarded to be contributed mostly from vanadia species. The number of acid sites was greatly increased by the addition of molybdenum species; acid sites for VMoT are about three times that for VT. These observations are consistent with the

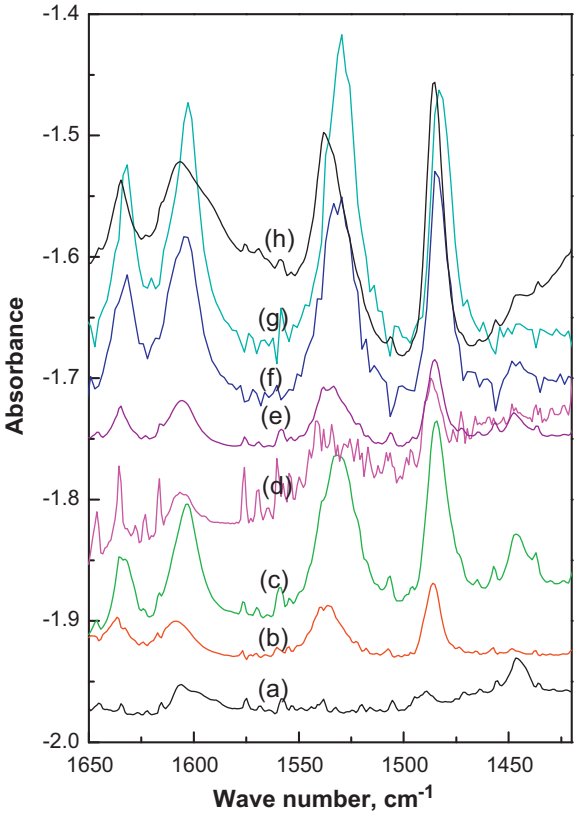

Fig. 7. FT-IR spectra of pyridine adsorbed on (a) anatase TiO_2, (b) VT, (c) VMoT, (d) UVT, (e) UVMoT, (f) SUVT, (g) SUVMoT, and (h) M_2O_3–TiO_2.

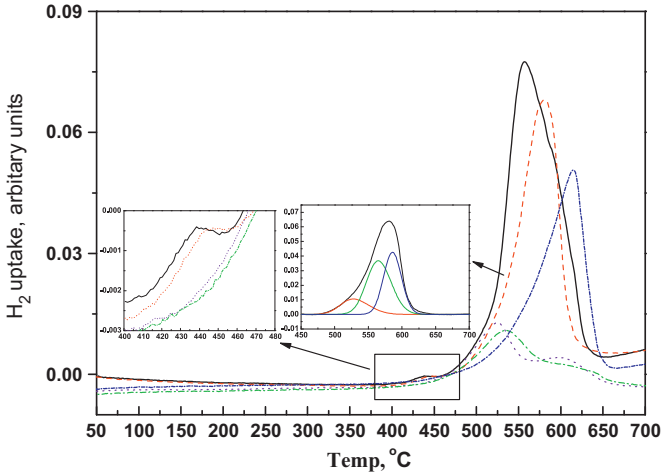

Fig. 8. Temperature programmed reduction characterizing VMoT (solid black line), UVMoT (red dash line), VT (blue dot line), and UVT (green dash dot line). (For interpretation of the references to color in this figure legend, the reader is referred to the web version of the article.)

reported data [17–19]. Correlating the Py-ads IR analysis with Rietveld refinement results, the numbers of acid sites are mostly contributed from amorphous vanadia; almost all vanadia species on VMoT are in amorphous form while only 35% of that are on VT. After the test reactions, the acid sites on VMoT are greatly reduced while those on VT have no significant change. Since synchrotron PXRD has indicated that the amorphous vanadia reacts with MoO_3 to form MoV_2O_8 with crystalline size of 25 nm, the reduction of acid sites may be caused by the loss of surface vanadia species.

In sulfur-oxides containing environment, the used catalysts present larger acid sites (both Lewis acid sides and Brønsted acid sites) than those catalysts ran in sulfur-oxides free environment [17–19]. The increase in acid sites is induced by the adsorption of sulfur oxides [44,45]. These increases in acid sites may enhance nucleophilic substitution of the aromatic chloride in the initial step of the reaction, leading to an increase of reaction rate [43,46].

Compared to MoVT, SUVT has more acid sites whereas presents slightly lower conversion and total oxidation selectivity at start of run (Fig. 1). According to the report by Albonetti et al. [16] that 1,2-dichlorobenzene conversion can be enhanced by the increase of Brønsted acid sites while Lewis acid sites enhance the further oxidation of the partial oxidation by-product. The higher selectivity to CO_2 for MoVT may be due to the higher Lewis to Brønsted acid sites ratio.

As shown in Eqs. (1) and (1), 2-dichlorobenzene conversion is dominated by *ko*, *Es*, and *Ha*. The slightly higher conversion for MoVT may be due to the presence of layer V_2O_5 which have lower activation energy for surface reaction.

3.6. Reducibility of VT, VMoT, UVT, and UVMoT

TPR profiles of VT, VMoT, UVT, and UMoT show the reduction temperatures of these four catalysts are different (Fig. 8). Two peaks appearing at 535 and 600 °C were observed for VT sample. Since the T_{max} value of TiO_2 supported vanadia catalysts is sensitive to support [47] and the morphology of vanadia species [48,49], the T_{max} value of these vanadia species is in the order of bulk V_2O_5 > polymeric V_2O_5 > isolated vanadia species [48,49]. Based on Rietveld refinement results, the peak at 535 °C and 600 °C are assigned as the reduction of small V_2O_5 clusters (polymeric) and crystalline (bulk) V_2O_5, respectively. After 1,2-dichlorobenzene oxidation reaction, the TPR peak at 535 °C shifts to higher temperature suggesting that the oxidation induces the aggregation of V_2O_5 clusters.

For VMoT catalyst, besides an asymmetry peak appearing at 575 °C, a rather small peak also appears at about 440 °C. The asymmetry peak at 575 °C is a lump of the reduction characteristic of the amorphous V_2O_5 and MoO_3 crystal. The shift of MoO_3 characteristic peak to lower temperature for VMoT may be caused by the co-catalytic reduction of V_2O_5.

After test reaction, the TPR profile also shifts to higher temperature, and the peak with T_{max} appearing at 580 °C can be decoupled into 3 peaks. The peaks at 535 and 560 °C are assigned to the reduction of V_2O_5 clusters and MoV_2O_8, respectively, while peak at 590 °C is assigned to the reduction of MoO_3. Since the reduction temperature of MoV_2O_8 is about 25 °C higher than that of V_2O_5 clusters while 40 °C lower than that of V_2O_5 crystal, the average reduction temperature of vanadia species for UVMoT is lower than that for UVT. The slightly lower activation energy for the oxidation of 1,2-dichlorobenzene catalyzed by VMoT may be caused by the slightly higher redox capability of MoV_2O_8. In addition, inferred from FT-IR results and the report of Bond [48], the rather small peak at about 440 °C may be the characteristic peak for the reduction of layer V_2O_5. The ease of the redox capability for the layer V_2O_5 may also be responsible for the decrease of the activation energy.

It has been reported that the catalytic enhancement of adding MoO_3 is mainly due to the effect by increases in acidity (Brønsted sites) [18,19]. In our study, decrease of acidity of UVMoT (as compared to VMoT) was observed, and it should results in a negative effect of the catalytic reactivity. However, the better dispersion of V (more layer V_2O_5 and polymeric V_2O_5) in UVMoT and the ease of the redox capability (lower activation energy for the oxidation of 1,2-dichlorobenzene) for layer V_2O_5, polymeric V_2O_5 and MoV_2O_8 result in a higher reactivity of the catalyst. Thus, the formation of MoV_2O_8 which results in a better dispersion of V_2O_5 under the catalytic reaction condition may be the intrinsic reason for the promotion of the catalytic activity in VMoT.

4. Conclusion

Rietveld refinement and FT-IR results show that the addition of MoO_3 to V_2O_5/TiO_2 catalysts greatly influences the structure of vanadia species. With the absence of MoO_3, about 65% of crystalline V_2O_5 and 35% V_2O_5 clusters are formed on TiO_2 supports. MoO_3 disperses vanadia on TiO_2 surface. With the presence of MoO_3, no crystalline V_2O_5 have been found and both 3-dimensional V_2O_5 clusters and 2-dimensional layer V_2O_5 are suggested to be formed on TiO_2–MoO_3 supports. The increase of V_2O_5 dispersion causes the increase of catalyst acidity and redox capability and leads to an increase of catalyst activity and selectivity. The amorphous V_2O_5 are very reactive to MoO_3, and about 90% of crystalline MoV_2O_8 have been found after test reaction.

References

[1] D.A. Bulushev, L. Kiwi-Minsker, V.I. Zaikovskii, A. Renken, J. Catal. 193 (2000) 145.
[2] D. Rohan, B.K. Hodnett, Appl. Catal. A: Gen. 151 (1997) 409.
[3] D. Heinz, W.F. Hoelderich, S. Krill, W. Boech, K. Huthmacher, J. Catal. 192 (2000) 1.
[4] E.M. Alkaeva, T.V. Andrushkevich, G.A. Zenkovets, M.G. Makarenko, United State Patent No. 5,728,837 (1998).
[5] D. Heinz, W. Holderich, S. Krill, W. Bock, United State Patent No. 6,229,018 B1 (2001).
[6] C.E. Hetrick, F. Patcas, M.D. Amiridis, Appl. Catal. B 101 (2011) 622.
[7] J.S. Jurng, G.N. Bae, K.H. Ahn, J.Y. Kim, H. Chung, United State Patent No. 0,054,231 (2009).
[8] J.S. Jurng, G.N. Bae, K.H. Ahn, J.Y. Kim, H. Chung, United State Patent No. 0,123,353 (2009).
[9] N. Sugishima, A. Morits, M. Kobayashi, United State Patent No. 6,120,747 (2009).
[10] F. Cavani, G. Centi, F. Parrinello, F. Trifirò, Preparation chemistry of V–Ti–O mixed oxides. Comparison of coprecipitation, grafting andimpregnation

methods, in: B. Delmon, P. Grange, P.A. Jacobs, G. Poncelet (Eds.), Preparation of Catalysts IV, Stud. Surf. Sci. Catal., vol. 31, Elsevier Science, Amsterdam, 1987, pp. 227–240.
[11] Y. Liu, Z. Wei, Z. Feng, M. Luo, P. Ying, C. Li, J. Catal. 202 (2001) 200.
[12] L. Lietti, I. Nova, G. Ramis, L.D. Acqua, G. Busca, E. Giamello, P. ForZatti, F. Bregani, J. Catal. 187 (1999) 419.
[13] J. Papp, S. Soled, K. Dwight, A. Wold, Chem. Mater. 6 (1994) 496.
[14] E. Finocchio, G. Ramis, G. Busca, Catal. Today 169 (2011) 3.
[15] D.P. Debecker, R. Delaigle, K. Bouchmella, P. Eloy, E.M. Gaigneaux, P.H. Mutin, Catal. Today 157 (2010) 125.
[16] S. Albonetti, J. Epoupa Mengou, F. Trifirò, Catal. Today 119 (2007) 295.
[17] F. Bertinchamps, C. Gregoire, E.M. Gaigneaux, Appl. Catal. B 66 (2006) 1.
[18] F. Bertinchamps, C. Gregoire, E.M. Gaigneaux, Appl. Catal. B 66 (2006) 10.
[19] D.P. Debecker, F. Bertinchamps, N. Blangenois, P. Eloy, E.M. Gaigneaux, Appl. Catal. B 74 (2007) 223.
[20] S. Krishnamoorthy, M.D. Amiridis, Catal. Today 51 (1999) 3.
[21] S. Krishnamoorthy, J.P. Baker, M.D. Amiridis, Catal. Today 40 (1998) 39.
[22] J.E. Lee, J. Jurng, Catal. Lett. 120 (2008) 294.
[23] D.P. Debecker, R. Delaigle, P. Eloy, E.M. Gaigneaux, J. Mol. Catal. A 289 (2008).
[24] D.P. Debecker, R. Delaigle, P.C. Hung, A. Buekens, E.M. Gaigneaux, M.B. Chang, Chemosphere 82 (2011) 1337.
[25] S. Krishnamoorthy, J.A. Rivas, M.D. Amiridis, J. Catal. 193 (2000) 264.
[26] A.P. Hammersley, ESRF Internal Report, FIT2D V12.012 Reference Manual, V6.0 ESRF98HA01T, 2004.
[27] H.M. Rietveld, J. Appl. Cryst. 2 (1969) 65.
[28] B.H. Toby, J. Appl. Cryst. 34 (2001) 210.
[29] A.C. Larson, R.B. Von Dreele, General Structure Analysis System (GSAS), Los Alamos National Laboratory Report LAUR, 2000, pp. 86–748.
[30] B.D. Cullity, Elements of X-Ray Diffraction, 2nd ed., Addison Wesley Publishing Company, Massachusetts, 1978, pp. 99–106.
[31] A. Jones, B. McNicol, Temperature-Programmed Reduction for Solid Materials Characterization, Marcel Dekker Inc., 1986.
[32] G.F. Froment, K.B. Bischoff, Chemical Reactor Analysis and Design, John Wiley & Sons, Inc., 1990, pp. 61–82.
[33] J. Lichtenberger, M.D. Amiridis, J. Catal. 223 (2004) 296.
[34] L. Seguin, M. Figlarz, R. Cavagnat, J.-C. Lassègues, Spectrochim. Acta A 51 (1995) 1324.
[35] L.-Q. Mai, W. Chen, Q. Xu, Q.-Y. Zhu, Microelectron. Eng. 66 (2003) 199.
[36] G. Busca, G. Centi, L. Marchetti, F. Trifirò, Langmuir 2 (1986) 568.
[37] S. Kataoka, E. Lee, M.I.T. -Tejedor, M.A. Anderson, Appl. Catal. B: Environ. 61 (2005) 159.
[38] K. Nakamoto, Infrared and Raman Spectra of Inorganic and Coordination Compounds, John Wiley, New York, 1997.
[39] X. Zhang, G. Zhuang, J. Chen, Y. Wang, X. Wang, Z. An, P. Zhang, J. Phys. Chem. B 110 (2006) 12588.
[40] Y.-X. Jiang, X.-M. Chen, Y.-F. Mo, Z.-F. Tong, J. Mol. Catal. A: Chem. 213 (2004) 231.
[41] C.-H. Lin, H. Bai, Appl. Catal. B: Environ. 42 (2003) 279.
[42] A. Sahibed-Dine, B. Bouanis, K. Nohair, M. Bensitel, Ann. Chim. Sci. Mater. 23 (1998) 139.
[43] S. Albonetti, S. Blasioli, R. Bonelli, J.E. Mengou, S. Scire, F. Trifirò, Appl. Catal. A: Gen. 341 (2008) 18.
[44] H. Zhao, S. Bennici, J. Shen, A. Auroux, J. Mol. Catal. A: Chem. 309 (2009) 28.
[45] X. Wang, J.C. Yu, P. Liu, X. Wang, W. Su, X. Fu, J. Photochem. Photobiol. A: Chem. 179 (2006) 339.
[46] M. Taralunga, J. Mijoin, P. Magnoux, Catal. Commun. 7 (2006) 115.
[47] I.E. Wachs, B.M. Weckhuysen, Appl. Catal. A: Gen. 157 (1997) 67.
[48] G.C. Bond, Appl. Catal. A: Gen. 157 (1997) 91.
[49] D.A. Bulushev, L. Kiwi-Minsker, F. Rainone, A. Renken, J. Catal. 205 (2002) 115.